Elena Garcia
Pablo Gonzalez de Santos

Industrial Automation Institute (CSIC)
28500 Madrid, Spain

Carlos Canudas de Wit

Laboratoire d'Automatique de Grenoble
38 402 St. Martin d'Hères, France

Velocity Dependence in the Cyclic Friction Arising with Gears

Abstract

Recent research on friction in robot joints and transmission systems has considered meshing friction a position-dependent friction component. However, in this paper we show experimental evidence that meshing friction depends highly on joint speed. We identify the meshing friction in the gearboxes of a robotic leg, and we propose a new mathematical model that considers the rate dependency of meshing friction. The resulting model is validated through experimentation. Results show that meshing friction is responsible for friction torque oscillations with an amplitude up to 25 percent of the average friction torque at low speeds. Therefore, this friction component should be taken into account if an accurate friction model is desired.

KEY WORDS—meshing friction, position-dependent friction, friction identification, friction modelling

1. Introduction

Friction in robotic systems is a source of path tracking imperfections that turn into steady-state errors and tracking lags. In the last century, extensive research was carried out to understand friction phenomena (Stribeck 1902; Bowden and Tabor 1956; Czichos 1978; Suh and Sin 1981; Armstrong-Helouvry 1991; Williams 1994), and static and dynamic friction models have been developed (Dahl 1968; Karnopp 1985; Haessig and Friedland 1991; Bliman 1992; Bliman and Sorine 1993; Harnoy and Friedland 1993; Armstrong-Helouvry et al. 1994; Canudas de Wit et al. 1995). Studies and models have been particularly devoted to friction in robotic systems, where motor drives and ball bearings have been the main sources of friction studied (Dahl 1968; Haessig and Friedland 1991; Armstrong-Helouvry 1991; Leonard and Krishnaprasad 1992; Armstrong-Helouvry et al. 1994), while friction in transmission systems is the subject of more recent exploration (Anderson and Lowenthal 1982; Armstrong 1988; Canudas de Wit et al. 1991; Phillips and Ballow 1993; Dohring et al. 1993; Popovic and Goldenberg 1998; Canudas de Wit and Praly 1998; Tahboub and Asada 2000).

Some specific robotic systems require high gearing for exerting high torques at the end-effector. This is the case of walking robot legs, which require high torques but need to use small actuators. This restriction means that high reduction ratios must be used in leg transmission systems, but as a consequence backlashes, elasticity and gear-specific friction components are generated.

Small imperfections on transmission system shafts generate position-dependent friction. As a result, small oscillations with the frequency of the reduction ratio appear. However, such oscillations do not modify more than 5% of the maximum friction torque (Armstrong 1988). Position-dependent friction was first modeled by Armstrong-Helouvry (1991) by means of a sinusoidal function of joint position. Thus, this friction component does not depend on joint speed.

Recent research on spur and helical gear dynamics claims that another source of position-dependent friction exists in the coming together of gear teeth (Shing 1994; Hochmann and Houser 2000). While power is transmitted along the line-of-action direction, friction occurs along the off line-of-action direction, which lies orthogonal to the line of action. The reason for this friction is that teeth slide together instead of rolling perfectly. Therefore, meshing friction is a source of inefficiency in gearboxes.

Anderson and Lowenthal (1982), studying gearing efficiency, concluded that sliding friction accounts for most of the losses at low speeds (pinion speed less than 250 rpm). This suggests some rate dependency in meshing friction, which distinguishes it from a position-dependent component.

This paper is specially devoted to studying these phenomena. In this paper, the friction components in the joints of a robotic leg have been determined experimentally. The testbed used for this purpose was the leg of the SILO4 walking robot (see Figure 1) (Galvez et al. 2000). Experimental evidence is

The International Journal of Robotics Research
Vol. 21, No. 9, September 2002, pp. 761-771,

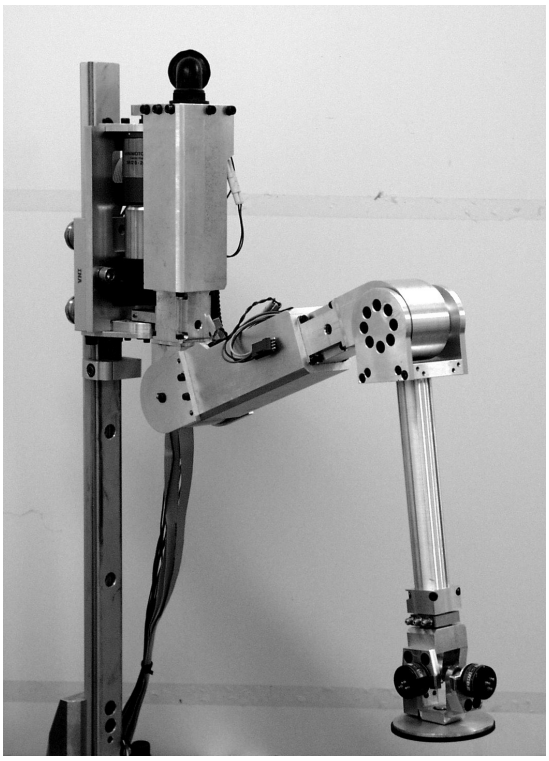

Fig. 1. Leg prototype used for friction identification.

given, suggesting that the amplitude of the torque oscillations caused by friction in gear teeth decreases exponentially with joint speed. Therefore, friction at meshing teeth is not only a position-dependent friction component as stated above. A new mathematical model for this friction considering its rate dependency is also proposed and validated with real friction data. In this paper, by the term "meshing friction" we refer to the rate-dependent friction occurring in meshing teeth instead of the position-dependent friction component caused by shaft eccentricities.

This paper is organized as follows. In Section 2 we describe the experimental testbed, and in Section 3 we describe the different experiments carried out in order to identify the friction components and meshing friction. A new mathematical model is proposed for meshing friction and parameter estimation is established in Section 4. The resulting friction model is validated in Section 5, and relevant results are discussed finally in Section 6.

2. Experimental Testbed

Different experiments have been carried out to identify the main friction components affecting the behavior of a three-degrees-of-freedom (3-DoF) rotational leg. Friction torques were determined for each joint of the leg by means of armature current measurement. For this purpose, links were removed from their joints to ensure there were no loads to increase the torque measurement. Armature current was sensed while each joint was moving at a constant speed in order to avoid exciting dynamic friction components. The torque value was then computed using the following equation:

$$\tau = k_M I_{av}, \tag{1}$$

where k_M is the torque constant and I_{av} is the average motor current. Assuming constant speed and no load affecting the motion, the computed torque becomes the friction torque. However, due to the waveform of the friction torque, it is very difficult to achieve a constant joint speed. Some inertial effects will therefore arise. Thus, friction is obtained by extracting the load inertia from the measured torque, that is

$$F = \tau - J\ddot{\theta}, \tag{2}$$

where F is the friction torque, J is the equivalent inertia of rotor and gearing, and θ is the joint position.

Figure 1 shows the leg prototype used in these experiments. Three servo-controlled DC motor drives provide motion to the three rotational joints of the leg. The pulse width modulation technique (PWM) is used to control the power supply of the motors. A 500-pulse-per-revolution optical encoder is attached to the motor drive to transmit joint positions to the controller. The control card, containing a digital proportional, integral, derivative (PID) filter, is connected to a host computer based on a 500-MHz Pentium PC. The PID filter controls both joint position and velocity at a rate of 16 KHz. Mechanical power is transmitted to the joints through planetary gearing and, in the case of the second and third joints of the leg, a skew-axis worm gear provides a transformation of 90 degrees to the transfer direction (see Figure 2). Table 1 contains reduction ratios of each gear stage in the leg joints, which will be referred to more fully below. The third joint was chosen for the experimental procedure because it has a complex mechanical transmission system containing two different gear stages, and link removal is easier here than at other joints.

A power meter is used to measure the armature current. The average value of the current, displayed by the power meter, is sampled at four milliseconds. To avoid aliasing effects (due to the 16-KHz component from the PWM), the power meter uses a 1-KHz fourth-order Bessel analog filter.

Finally, the average current data is collected in a host computer, where eq. (2) is computed.

A warm-up procedure was performed previous to the experiments to avoid the dwell effect (friction is sensitive to temperature) (Armstrong-Helouvry 1991). This procedure consisted of several rotations of the joint at top speed in both directions. Ten experiments were then performed for each joint speed, and the mean of all of these was used for friction identification. Good repetitiveness of the experiments was achieved with less than 3% standard deviation from the mean.

Table 1. Gear Reduction Ratios for the SILO4 Leg

Gear box type	Joint 1	Joint 2	Joint 3
Planetary	246	14	14
Spiroidal skew-axis	—	20.5	20.5

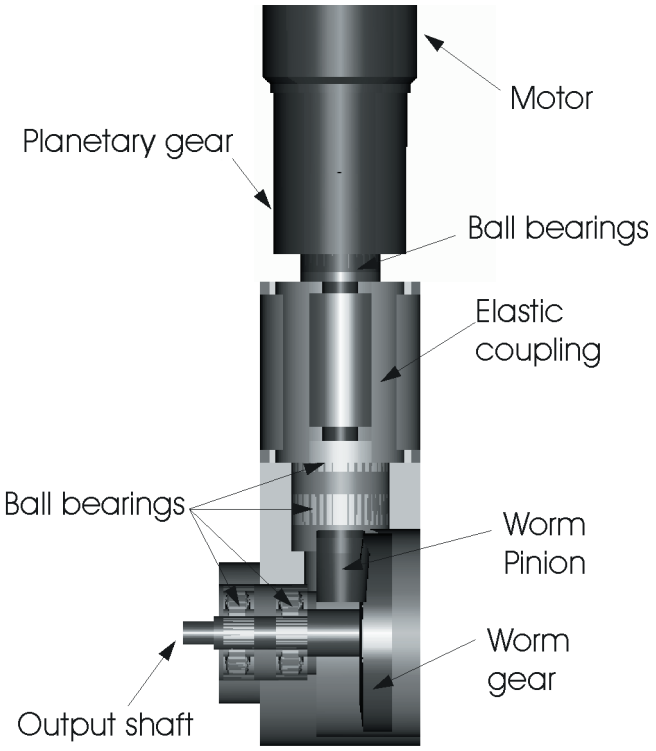

Fig. 2. Sectioned model of the joint drive and transmission system configuration.

3. Experimental Identification of Friction

The aim of this research is to identify the friction components affecting leg dynamics. There are different sources of friction inside the complex mechanical structure of a leg, as mentioned above. Gearboxes, ball bearings and shaft imperfections all contribute different friction components. The experiments performed in order to identify the main friction components affecting leg joint motion were carried out by removing the link load and keeping the whole mechanical transmission system complete. The main friction components found are explained in the following subsections. First, friction components at low velocities are identified, and models taken from Canudas de Wit et al. (1991) are used. Subsequently, position-dependent and meshing friction are identified by the spectral analysis technique, previously used by Popovic and Goldenberg (1998).

3.1. Friction at Low Velocities

Stiction takes place at zero speed due to the static friction torque, which fights motion. The controller must maintain a commanded speed, and thus a stick-slip effect is created. Figure 3 shows this behavior. Although the controller commands the joint to rotate at a constant speed of approximately 0.0001 rad/s, the measured joint speed undergoes impulsive decrements due to small increments in the friction torque (i.e., at the joint position of 0.0182 and 0.022 radians). Also, when this friction decreases, the joint speed increases until the controller acts (i.e., at the joint position of 0.021 and 0.0222 radians). Note that cogging effects due to graphite commutation are apparent at low speeds, as shown in Figure 3. However, the amplitude of these effects can be neglected. The oscillations caused by meshing friction are very high at these low speeds, and the amplitude of cogging effects represents less than 1% of the meshing friction amplitude.

The average stiction torque can be identified along with the Stribeck effect and Coulomb and viscous components. These friction components affecting joint motion were determined by collecting the average friction measured at a range of motor speeds. Figure 4 shows the resulting curve, known as the Stribeck curve at low velocities.

Parameter identification was performed using the least-squares technique. The static plus Stribeck plus Coulomb plus viscous friction model is known to be (Canudas de Wit et al. 1991):

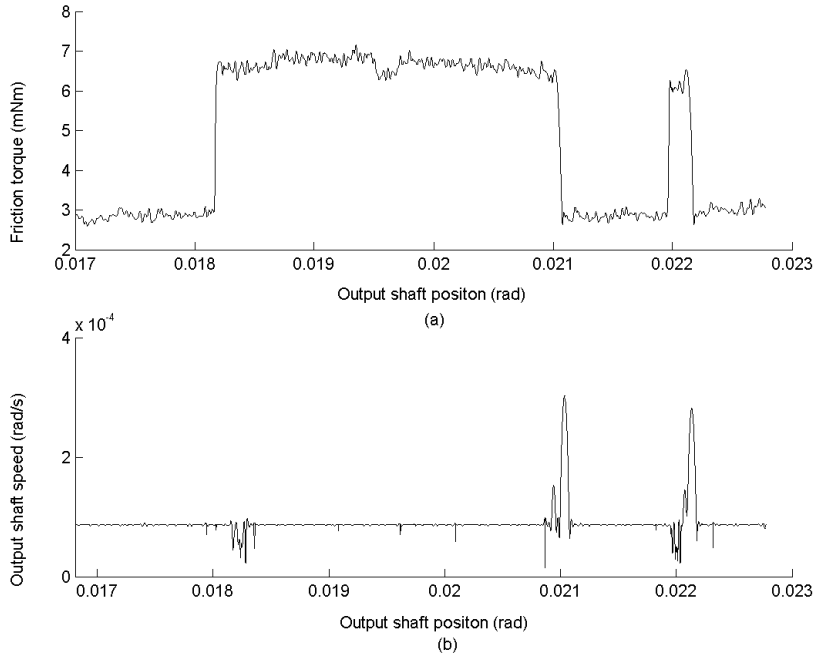

Fig. 3. Stick-slip effect at low joint velocity.

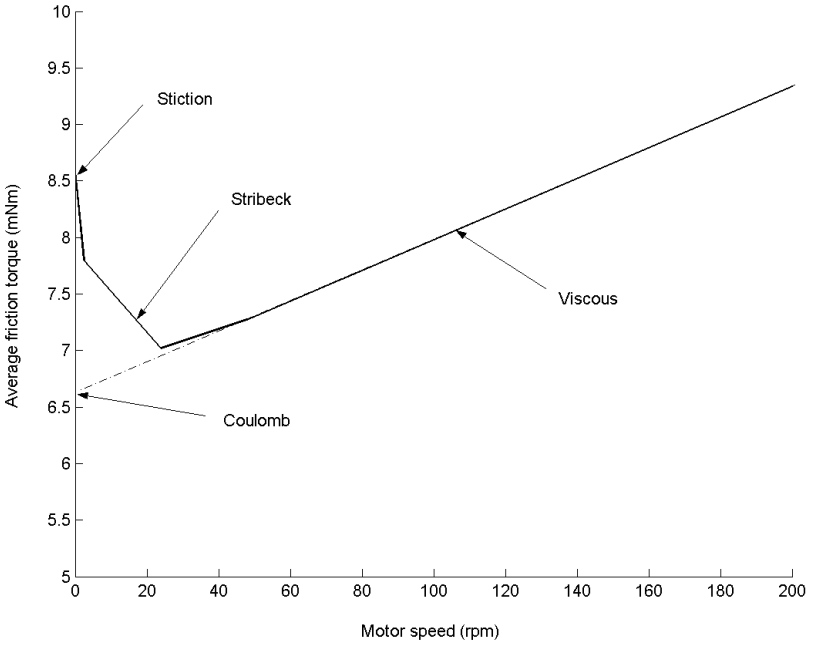

Fig. 4. Curve of average friction torque versus motor velocity, which reflects the friction components at low speeds.

$$\tau_f\left(\dot{\theta}\right) = \left[\tau_C + (\tau_E - \tau_C)e^{\frac{-\left|\dot{\theta}\right|}{\dot{\theta}_s}} + B\left|\dot{\theta}\right|\right]\text{sign}\left(\dot{\theta}\right), \qquad (3)$$

where τ_E is the static friction, τ_C is the Coulomb friction, B is the viscosity coefficient, and $\dot{\theta}_s$ is the Stribeck velocity. If we extract the experimental friction data corresponding to motor speeds high enough to avoid the Stribeck effect (over 100 rpm), τ_C and B can be estimated by neglecting the exponential term.

τ_E and $\dot{\theta}_s$ are identified by considering the experimental data from very low velocities. Then, the viscous term in eq. (3) can be neglected. Manipulating the resulting expression yields:

$$\ln(\tau_f - \tau_C) = \ln(\tau_E - \tau_C) - \frac{|\dot{\theta}|}{\dot{\theta}_s}. \qquad (4)$$

As τ_f and τ_C are already known, the above expression is of the form

$$y = m\left|\dot{\theta}\right| + n, \qquad (5)$$

where $m = -1/\dot{\theta}_s$, $n = \ln(\tau_E - \tau_C)$ and $y = \ln(\tau_f - \tau_C)$. After m and n are estimated by the least-squares regression method, the static friction value and the Stribeck velocity can be estimated. The estimated parameters are listed in Table 2.

3.2 Position-dependent Friction

The most significant friction effect observed during these experiments was the oscillatory shape of friction torque. Armstrong-Helouvry (1991), Canudas de Wit et al. (1991), Canudas de Wit and Ge (1997), and Canudas de Wit and Praly (1998) pointed out that imperfections on the shaft and gearing centers generate torque oscillations with a period equal to the gear reduction ratio. This position-dependent friction does not depend on joint speed, and it has been modeled as a sinusoidal wave with the frequency of the gearbox. Experiments performed in industrial manipulators have shown that this position dependence is relatively weak, modifying no more than 5% of the maximum absolute value of friction (Armstrong 1988).

In order to verify that such position-dependent friction exists in the joints of a walking robot, friction torque was plotted versus joint position as shown in Figure 5. Spectral analysis of the measured friction torque versus joint position along the whole range of motor speeds reflected three spectral components, corresponding, as predicted, to joint, worm gear pinion and motor shaft rotation frequency, respectively. That is, the lowest spectral component, $F_1 = 0.159$ cycles/rad, corresponded to one output joint shaft rotation ($\omega_1 = 2\pi F_1 = 1$). The next spectral component, $F_2 = 3.26$ cycles/rad, corresponded to the worm gear reduction ratio ($\omega_2 = 2\pi F_2 = 20.5$). The highest spectral component, $F_3 = 45.6$ cycles/rad, matched planetary gearbox reduction ($\omega_3 = 2\pi F_3 = 287$) (see Figure 6). The oscillations at frequency F_1 maintained the same amplitude for all three motor speeds shown in the figure. However, as Figure 5 and 6 show, the amplitude of oscillations at frequencies F_2 and F_3 decreased as motor speed increased. This observation does not match the definition of position-dependent friction, which previous authors have assumed to be rate-independent (Armstrong-Helouvry 1991; Canudas de Wit et al. 1991; Phillips and Ballow 1993; Popovic and Goldenberg 1998).

The significance of the oscillations at frequencies F_2 and F_3 can be observed in Figure 7. The amplitude of friction oscillations at F_2 becomes more than 25 percent of the average friction at low speeds (see Figure 7(a)). On the other hand, the amplitude of oscillations at F_3 becomes 4% of the average friction at low velocities (see Figure 7(b)). Both figures show an exponential decrease of the oscillation amplitude with joint speed. Therefore, only torque oscillations at frequency F_1 match the definition of position-dependent friction.

Position-dependent friction is usually modeled as a sinusoidal wave with constant amplitude. Although in our opinion this type of friction also depends on the load, it is currently modeled only as a function of motor speed, as in Canudas de Wit et al. (1991). Future work will aim at modeling this friction component as a function of the load. The model used at present is represented by

$$\tau_f(\theta) = A_1 \sin(\omega_1\theta + \varphi_1), \qquad (6)$$

where A_1 represents the oscillation amplitude and depends on the stiffness of the ball bearings and the deflection caused by shaft imperfections. The oscillation frequency is represented by ω_1, and lastly φ_1 is the phase of the oscillations.

An estimation of parameters A_1, ω_1 and φ_1 for the position dependence at frequency F_1 is obtained from spectral analysis. The resulting values are given in Table 2.

3.3. Meshing Friction

Meshing friction and ball bearing deflection are another source of friction torque oscillations (Popovic and Goldenberg 1998; Hochmann and Houser 2000). Although this type of friction has been considered position-dependent, recent research in spur and helical gearing dynamics (Anderson and Lowenthal 1982; Shing 1994; Hochmann and Houser 2000) has predicted differences between meshing friction and position-dependent friction. Power and load in gear trains are transmitted along the line of action. The relative reduced stiffness of shaft support ball bearings may be responsible for small shaft displacements along the line-of-action direction, which would cause torque oscillations; this is called position-dependent friction. However, the meshing friction force in gear teeth is transmitted in the off line-of-action direction. It

Table 2. Parameters Identified in the Friction Model

	τ_E (mNm)	τ_C (mNm)	θ_s (rpm-motor)	B (mNm/rpm)
Positive	8.58	7.106	28.18	0.0134
Negative	9.41	7.909	26.58	0.0138
	A_1 (mNm)	ω_1 (rad/s)	ϕ_1 (rad)	
Positive	0.3	3.5×10^{-3}	$\pi/2$	
Negative	0.3	3.5×10^{-3}	$\pi/2$	
	A_2 (mNm)	b_2 (rpm-1)	ω_2 (rad/s)	ϕ_2 (rad)
Positive	0.576	1.27×10^{-4}	0.071	$\pi/2$
Negative	0.526	1.12×10^{-4}	0.071	$\pi/2$
	A_3 (mNm)	b_3 (rpm-1)	ω_3 (rad/s)	ϕ_3 (rad)
Positive	0.133	5.28×10^{-5}	1	π
Negative	0.152	7.49×10^{-6}	1	π

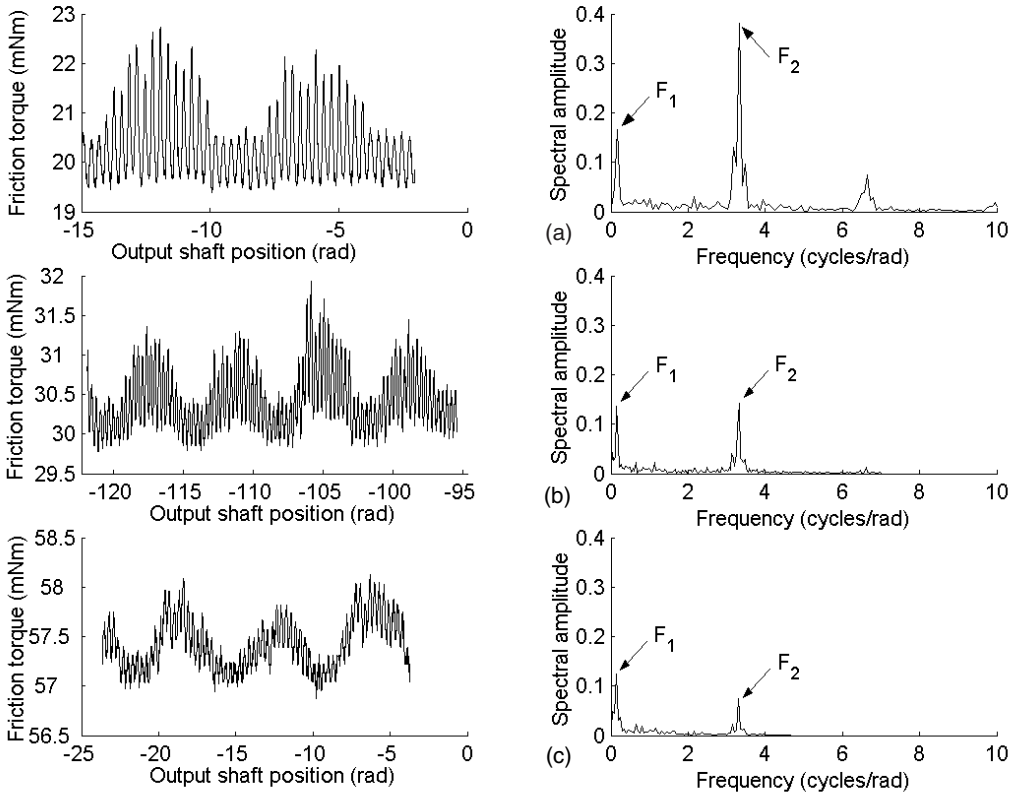

Fig. 5. Friction torque versus joint position and spectral analysis when the motor rotates at (a) 2000 rpm, (b) 4500 rpm, and (c) 6500 rpm.

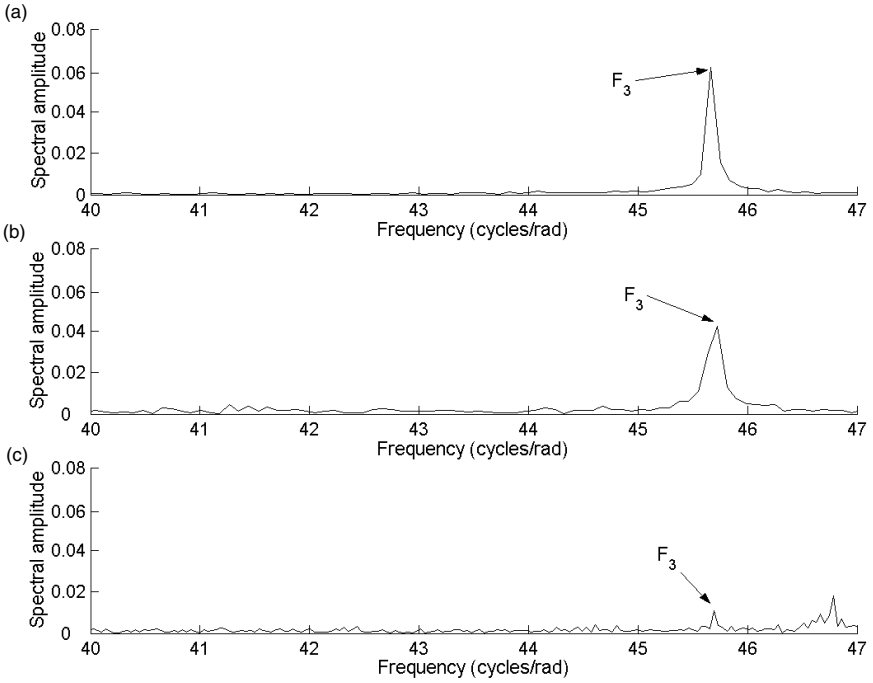

Fig. 6. Spectral component at F_3=45.6 cycles/rad when the motor rotates at (a) 2000 rpm, (b) 4500 rpm, and (c) 6500 rpm.

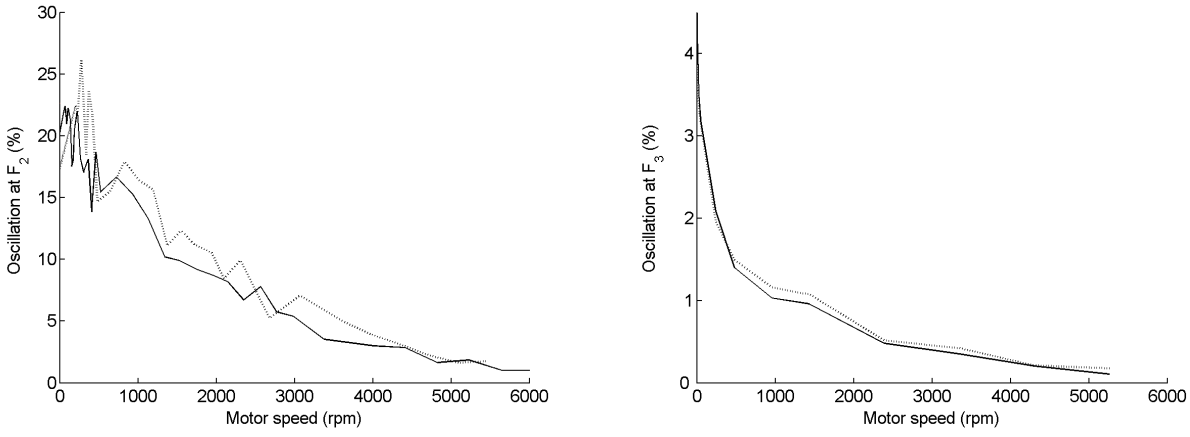

(a) (b)

Fig. 7. Percentage of torque oscillations when rotating forwards (solid line) and backwards (dotted line) at (a) F_2 and (b) F_3.

also causes shaft displacements due to the elastic deformation of ball bearings, but in this case the displacements are in the off line-of-action direction. There is experimental evidence that the motion in the off line-of-action direction may be several times larger than the motion in the line-of-action direction at gear mesh frequencies (Hochmann and Houser 2000). A dynamic study of the worm gear pair also reveals this same force arrangement (Garcia and Gonzalez de Santos 2001).

But why does meshing friction decrease exponentially with speed as shown in Figure 7? The friction coefficient between gear teeth depends heavily on lubricant properties, and it decreases as the relative sliding velocity between gear teeth increases (Henriot 1975). This is illustrated in Figure 8, which plots the typical curve of friction coefficient variation with sliding velocity in worm gears, with one lubricant based on vegetable oil and another based on mineral oil (taken from Henriot (1975)). The value of the sliding velocity, when worm and gear axes are orthogonal, is related to the angular velocity of the worm according to the following expression

$$v_l = \frac{r_1}{\sin \beta_1} \omega_1, \tag{7}$$

where v_1 is the sliding velocity, ω_1 is the worm angular velocity, r_1 is the primitive radius of the worm, and β_1 is the primitive inclination angle of the pinion with respect to its axis. Taking into account that r_1 and β_1 are constant, Figure 8 also reflects the relationship between friction coefficient and motor speed. Note the similarity in appearance between this curve and the experimental friction oscillation amplitude in Figure 7(a). Therefore, meshing friction is responsible for friction oscillations at frequencies F_2 and F_3.

Thus, there are two different friction components in the oscillatory behavior of friction. The first is a well-known component, position-dependent friction. The second is meshing friction, which has been found to be especially important at low speeds, where it reaches a 25% oscillation over the average friction in this case study. The amplitude of this oscillation will depend on lubricant, materials, and gear teeth and bearing stiffness. Both position-dependent friction and meshing friction will depend on the load, because the ball-bearing deflection depends on the load (Hochmann and Houser 2000), and so does friction in gear teeth (Henriot 1975). Therefore, the modeling of these two friction components should depend on load and speed.

The amplitude of the oscillation caused by meshing friction also depends on the gear type. The operating principle of spur or helical gears is rolling between teeth; thus, meshing friction could be small in some cases. However, the operating principle of other types of gears, such as worm gears, is almost pure sliding friction. While speed is low, the lubricant film is not enough to prevent contact between asperities, and friction becomes very high. As long as speed increases, the lubricant film will become sufficient to decrease friction. Thus, the amplitude of the oscillations caused by meshing friction depends heavily on gear type.

3.4. Asymmetries

Mechanical imperfections in the motor drive are known to be responsible for asymmetric behavior in friction torque. Transmission systems may also be responsible for such behavior. Asperities could be worn off in a particular direction of motion if the mechanical system moves typically in just one direction. Figure 7 is a comparison of meshing friction torque at increasing velocities when the joint rotates forwards (solid line) and backwards (dotted line). Figure 7(a) shows the asymmetric behavior of meshing friction at the worm gear (F_2), and Figure 7(b) shows asymmetries in meshing friction at the planetary gear (F_3).

4. A New Model of Meshing Friction

Meshing friction was not identified as a friction component separate from position-dependent friction in previous work on robot manipulators (Armstrong 1988; Phillips and Ballow 1993; Popovic and Goldenberg 1998; Tahboub and Asada 2000). Like position-dependent friction, the oscillations caused by meshing friction are modeled here as a sinusoidal wave; however, Figure 7(a) and (b) show that the amplitude of these oscillations decays exponentially with motor speed. Therefore, the model proposed here for meshing friction will contain a rate-dependent amplitude term. Meshing friction also produces ball-bearing deflection; therefore the amplitude of these oscillations will depend on bearing stiffness as well. The meshing friction model becomes

$$\tau_f\left(\dot{\theta}\right) = A_2 e^{-b_2|\dot{\theta}|} \sin(\omega_2 \theta + \varphi_2), \tag{8}$$

where A_2 represents the oscillation amplitude, and b_2 is the decay constant of the amplitude. Note that A_2 depends on the stiffness of gear teeth and ball bearings, respectively. The oscillation frequency is represented by ω_2, which corresponds to the reduction ratio. Finally, φ_2 is the oscillation phase. An estimate of parameters A_2, ω_2 and φ_2 for the meshing friction at frequencies F_2 and F_3 is obtained from spectral analysis. The decay constant b_2 is identified using the amplitude of the friction data

$$Ampl(\tau_f) = A_2 e^{-b_2|\dot{\theta}|}, \tag{9}$$

where the function *Ampl* returns the amplitude of the data given by spectral analysis. Manipulating the above expression, we achieve

$$\ln(Ampl(\tau_f)) = \ln(A_2) - b_2 \left|\dot{\theta}\right|, \tag{10}$$

where A_2 and b_2 are obtained by the least-squares method. The resulting values are given in Table 2.

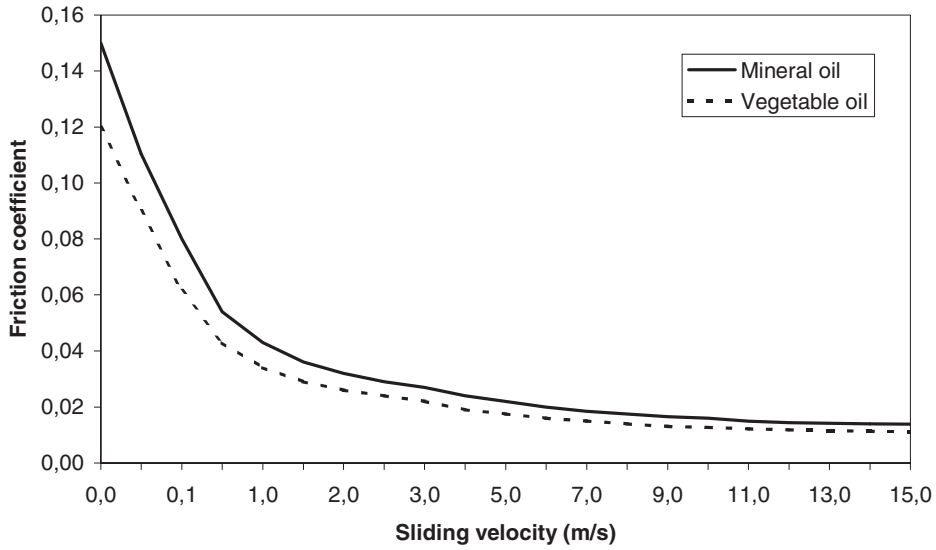

Fig. 8. Values of friction coefficient versus sliding velocity of worm gears with mineral oil-based lubricant and vegetable oil-based lubricant.

The complete joint friction model that integrates all the components herein identified is expressed in the following equation

$$\tau_f\left(\dot{\theta}\right) = \left\{\tau_C^i + (\tau_E^i - \tau_C^i)e^{\frac{-|\dot{\theta}|}{v_s}} + B^i\left|\dot{\theta}\right| + A_1^i \sin(\omega_1\theta + \varphi_1) + \sum_{k=2}^{3} A_k^i e^{-b_k|\dot{\theta}|}\sin(\omega_k\theta + \varphi_k)\right\} \operatorname{sign}\left(\dot{\theta}\right), \tag{11}$$

where subscript i denotes direction of motion (positive or negative), and k denotes the reduction stage. Table 2 gives all estimated parameters.

5. Model Validation

To determine the quality of the friction model thus obtained, a simulation of the model at different motor speeds was run and compared with real friction data, after which the model error was computed. Due to the wave shape of the model error, the average error and its standard deviation are given. The standard deviation is calculated as follows:

$$s(e) = \left(\frac{1}{n-1}\sum_{i=1}^{n}(e_i - \overline{e})^2\right)^{\frac{1}{2}}, \tag{12}$$

where

$$\overline{e} = \frac{1}{n}\sum_{i=1}^{n} e_i \tag{13}$$

is the average error and n is the amount of data.

Figure 9 shows model validation at three different motor speeds. The friction model and real data are compared as solid and dotted lines, respectively, for each motor speed. Table 3 lists average model error and standard deviation (or root mean square) figures for the same motor speeds. The average errors and standard deviations listed are 1.4% over the average friction for the lowest motor speed, 0.7% over the average friction for the next highest motor speed, and 0.3% under the average friction for the top motor speed. The absolute value of average error decreases with motor speed, and standard deviation decreases likewise. The average error is mostly influenced by the viscous friction model, while the standard deviation is influenced by the meshing friction model. Taking into consideration that model errors in dynamic models of robot manipulators can be up to 30% (they do not usually consider nonlinear dynamics as friction, backlash and elasticity), the average error and standard deviation presented here are sufficiently accurate for this application.

6. Future Work

Meshing friction also depends on the load due to tooth stiffness. Doring et al. (1993) have suggested that friction in worm gears may be dependent on the square of the load torque. This load dependency can be included in the meshing friction model in the oscillation amplitude term, that is

$$\tau_f\left(\dot{\theta}\right) = A_2(\tau_L^2)e^{-b_2|\dot{\theta}|}\sin(\omega_2\theta + \varphi_2), \tag{14}$$

where τ_L represents the load torque.

Table 3. Average Model Error and Standard Deviation

Motor Speed (rpm)	280	560	3000
s(e) (mNm)	0.21	0.17	0.12
$\bar{e}$ (mNm)	−0.17	−0.12	0.16

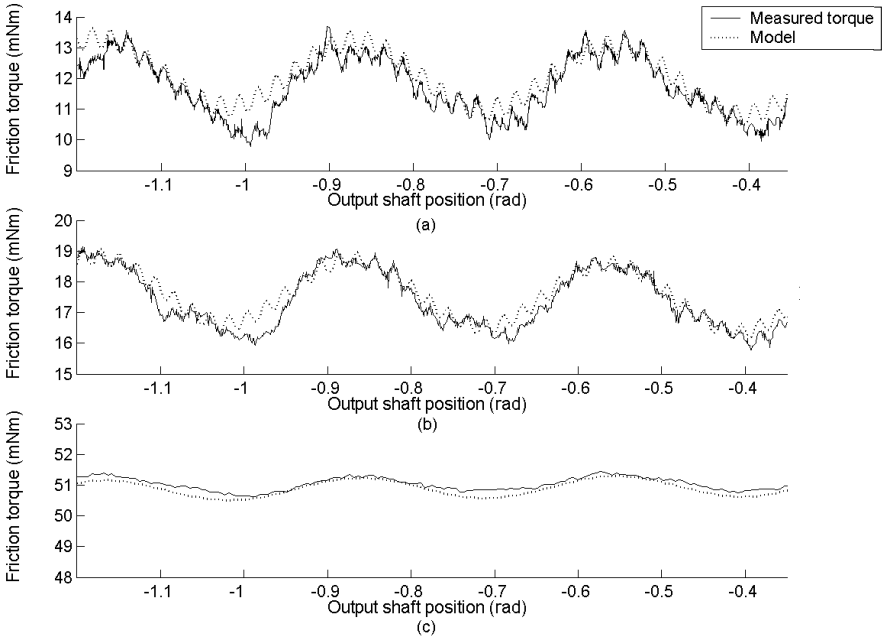

Fig. 9. Friction model validation. Comparison between real friction data (solid line) and model simulation (dotted line) for different motor speeds: (a) 280 rpm; (b) 560 rpm; (c) 3000 rpm.

However, this work provides no experimental justification of the expression (14) and therefore proposes a model of meshing friction as a function of motor speed only. Future work will involve the experimental identification of the load dependency of meshing friction.

7. Discussion

Robotic systems that need to provide high torques at the end-effectors usually contain high-reduction gears in their transmissions, causing some gear-specific friction components to appear, such as position-dependent friction.

Meshing friction in gear pairs has been defined in earlier works as a force along the off line-of-action direction that two paired teeth exert against each other while they match. As this force takes place once a pair of teeth comes together, it generates a periodic waveform friction with the frequency with which the two teeth match. For that reason it has been always considered position-dependent friction.

In the research presented here, it was experimentally found that meshing friction differs from position-dependent friction. The most important difference is the rate dependency of meshing friction. Spectral analyses show an exponential decrease of the meshing friction force as joint speed increases. This is an important and novel contribution. Meshing friction can be dominant at low speed and should be carefully modeled in systems involving slow motion, such as walking robots.

For this reason we have proposed a model of meshing friction. The model is similar to the position-dependent friction model, except for the variable amplitude of the sinusoidal wave.

Depending on material properties and gear type, meshing friction can become significant enough, and it will be taken into account if an accurate friction model is required. Our experiments show that the amplitude of the oscillations caused by meshing friction can account for up to 25 percent of the average friction torque at low speed.

Acknowledgments

EG would like to thank the Comunidad Autónoma de Madrid for funding her work and her stay at the Laboratoire d'Automatique de Grenoble.

References

Anderson, N. E. and Lowenthal, S. H. 1982. Design of spur gears for improved efficiency. *ASME J. Mech. Des.*, 104:767–774.

Armstrong, B. 1988. Friction: Experimental determination, modeling and compensation. *IEEE Int. Conf. on Robotics and Automation*, 3:1422–1427.

Armstrong-Helouvry, B. 1991. *Control of Machines with Friction.* Boston: Kluwer Academic.

Armstrong-Helouvry, B., Dumont, P., and Canudas de Wit, C. 1994. Survey of models, analysis tools and compensation methods for control of machines with friction. *Automatica* 30(7):1083–1138.

Bliman, P-A. 1992. Mathematical study of the Dahl's friction model. *Eur. J. Mech. A* 11(6):835–848.

Bliman, P-A. and Sorine, M. 1993. A system-theoretic approach of systems with hysteresis: application to friction modelling and compensation. *Proc. 2nd European Control Conf.*, Gronongen, The Netherlands. pp. 1844–1849.

Bowden, F. and Tabor, D. 1956. *Friction and Lubrication*. New York: Wiley.

Canudas de Wit, C., Noel, P., Aubin, A., and Brogliato, B. 1991. Adaptive friction compensation in robot manipulators: low velocities. *International Journal of Robotics Research* 10(3):189–199.

Canudas de Wit, C., Olsson, H., Aström, K. J., and Lischinsky, P. 1995. A new model for control of systems with friction. *IEEE Trans. Automatic Control* 40(3):419–425.

Canudas de Wit, C. and Ge, S. S. 1997 December 10-12. Adaptive friction compensation for systems with generalized velocity/position friction dependency. *Conf. on Decision and Control*, San Diego, CA, USA.

Canudas de Wit, C. and Praly, L. 1998. Adaptive eccentricity compensation. *37th IEEE Conf. on Decision and Control*, Tampa, Florida.

Czichos, H. 1978. *Tribology*. Amsterdam: Elsevier.

Dahl, P. 1968. A solid friction model. Technical Report TOR-0158(3107-18)-1, Aerospace Corporation, El Segundo, CA, USA.

Dohring, M. E., Eunjeong, L., and Newman, W. S. 1993. Load-dependent transmission friction model: Theory and experiments, *IEEE Int. Conf. on Robotics and Automation*, pp. 430–436.

Garcia, E. and Gonzalez de Santos, P. 2001 September 24-26. Relevant friction effects on walking machines. *Proc. 4th Int. Conf. on Climbing and Walking Robots*, Karlsruhe, Germany.

Galvez, J. A., Estremera, J., and González-de-Santos, P. 2000 October 2-4. SILO4: A versatile quadruped robot for research in force distribution. *Proc. 3rd Int. Conf. on Climbing and Walking Robots*, Madrid, Spain, pp. 371–383.

Haessig, D. A. and Friedland, B. 1991. On the modeling and simulation of friction. *J. Dyn. Syst. Meas. Control Trans. ASME* 113(3):354–362.

Henriot, G. 1975. *Traité Théorique et Pratique des Engrenages*. 5th edition. Dunod Publishers.

Harnoy, A. and Friedland, B. 1993. Dynamic friction model of lubricated surfaces for precise motion control. Preprint No 93-TC-1D-2. Society of Tribologists and Lubrication Engineers.

Hochmann, D. and Houser, D. R. 2000. Friction forces as a dynamic excitation source in involute spur and helical gearing. *Proc. DETC2000/PTG 8th Int. Power Transmission and Gearing Conf.*, Baltimore, MD, USA, pp. 10–13.

Karnopp, D. 1985. Computer simulation of stick-slip friction in mechanical dynamic systems. *J. Dyn. Syst. Meas. Control* 107(1):100–103.

Leonard, N. E. and Krishnaprasad, P. S. 1992. Adaptive friction compensation for bidirectional low-velocity position tracking, *Proc. 30th IEEE Conf. on Decision and Control*, New York, pp. 267–273.

Phillips, S. M. and Ballow, K. R. 1993. Friction modeling and compensation for an industrial robot, *J. Robotic Syst.* 10(7):947–971.

Popovic, M. R. and Goldenberg, A. A. 1998. Modeling of friction using spectral analysis, *IEEE Trans. Robotics Automation* 14(1):114–122.

Shing, T. K. 1994. Dynamics and control of geared servomechanisms with backlash and friction consideration. Ph.D. Thesis. The University of Maryland.

Stribeck, R. 1902. Die wesentlichen Eigenschaften der Gleitund Rollenlarger: The key qualities of sliding and roller bearings. *Z. Vereines Deutsch Ingen* 46(38,39):1342–1348, 1432–1437.

Suh, N. P. and Sin, H. C. 1981. The genesis of friction. *Wear* 69(1):91–114.

Tahboub, K. A. and Asada, H. H. 2000. Dynamics analysis and control of a holonomic vehicle with a continuously variable transmission, *IEEE Int. Conf. on Robotics and Automation*, San Francisco, CA, USA, pp. 2466–2472.

Williams, J. A. 1994. *Engineering Tribology*. Oxford: Oxford University Press.